Available online at www.sciencedirect.com
SCIENCE DIRECT®
Journal of the European Ceramic Society 25 (2005) 1119–1132
www.elsevier.com/locate/jeurceramsoc

Hertzian crack analysis in alumina–chromium composites

G. Geandier [a,*], S. Denis [b], A. Hazotte [c], A. Mocellin [b]

[a] *E.S.R.F. (European Synchrotron Radiation Facilities), 6 rue Jules Horowitz, BP 220 38043 Grenoble Cedex 9, France*
[b] *L.S.G.2M. (Laboratoire de Science et Génie des Matériaux et de Métallurgie), UMR CNRS INPL no 7584 Ecole des Mines de Nancy, Parc de Saurupt, 54042 Nancy Cedex, France*
[c] *L.E.T.A.M. (Laboratoire d'Etude des Textures Appliquées Aux Matériaux), UMR CNRS/Université de Metz no 7078, LETAM ISGMP, Ile de Saulcy, 57045 Metz Cedex 1, France*

Received 11 November 2003; received in revised form 2 April 2004; accepted 22 April 2004
Available online 3 July 2004

Abstract

Ceramic metal composites are of interest for their good resistance to crack propagation. We have prepared different kinds of alumina chromium composites, observed their microstructures and made an analysis of Hertzian cracks in order to identify the principle parameters of crack propagation in relation with the metallic phase size and distribution in the matrix. The crack is analysed at two scales, a macroscopic one to estimate the fracture toughness from the overall crack and a microscopic one to study, at the local level, the influence of the metallic phase on crack propagation. Using macroscopic models the fracture toughness estimation highlights the benefit of the presence of chromium particles. Observations and measurements made on the crack path and metallic phase, from the microstructure analysis, combined with the knowledge of the residual stress state, provide the principal parameters governing crack propagation in these composites.

Keywords: Ceramic Matrix Composite; Hertz crack; Fracture toughness; Microstructure; Al_2O_3/Cr

1. Introduction

Al_2O_3–metal composites are known for their improved mechanical properties as compared to pure alumina. Their production by hot pressing of mechanosynthesized nanocomposite powders allows obtaining dense, homogeneous ceramic-metal materials containing high metal contents.[1] The optimisation of the properties of these materials requires controlling the size and morphology of the reinforcing phase but also a good knowledge of the interaction between a propagating crack and the microstructure. In this work, we analyse Hertzian cracks made in alumina chromium composite which are heterogerenous material, to investigate their mechanical behaviours. The analysis takes into account all error sources due to specificity of the materials. Hertzian indentation is used for its experimental simplicity and well defined crack geometry compared to other techniques, such as Vickers indentation.[2] Hertzian indentation is also a technique that has not been tested on heterogenous materials. Results from indentations and micromechanical analysis[3] are used for the interpretation of relations between microstructure, mechanical state and crack paths in the composites.

The first part of the paper will describe the samples, their elaboration and a microstructural analysis of the different types of composites. The second part deals with the experimental set-up and a reminder of the Hertzian test. The third part presents the results of crack analysis at a macroscopic and a microscopic scale and analyses the crack propagation in relation with the microstructure and the local residual state of stress.

2. Sample preparation

The materials under study here are composites prepared by mechanical alloying.[1,4] The starting powders are metallic aluminium, alumina and chromium oxide. High-energy milling is carried out in a planetary ball mill with steel balls. This mechanical process allows to synthesize a chromium-alumina composite through the following reaction:

$$2Al + Cr_2O_3(+Al_2O_3) \rightarrow 2Cr + Al_2O_3$$

* Corresponding author.
E-mail address: geandier@esrf.fr (G. Geandier).

0955-2219/$ – see front matter.
doi:10.1016/j.jeurceramsoc.2004.04.022

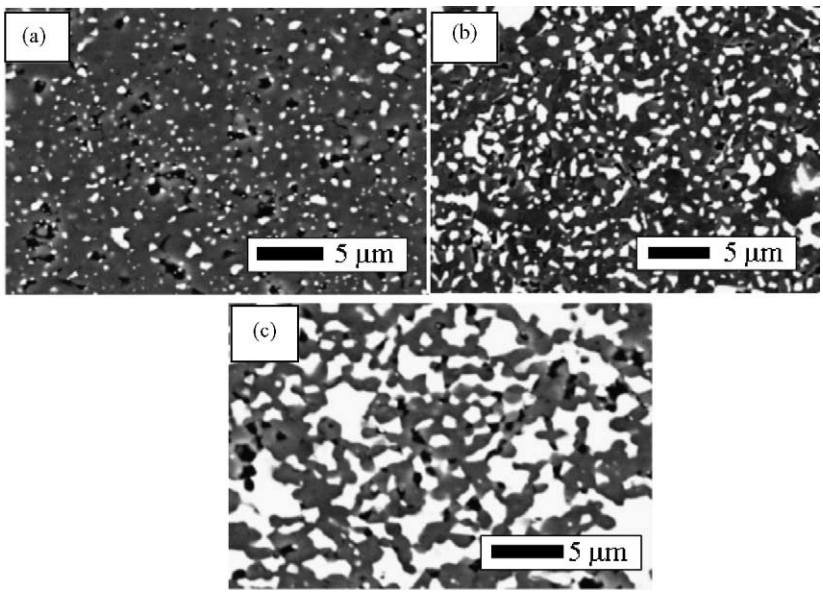

Fig. 1. SEM images of alumina chromium composites: (a) 9%, (b) 21%, and (c) 36% type I.

The proportion of powders is chosen to yield various volume fractions of metallic phase between 9 and 36%. In order to obtain dense samples, the powders are hot pressed in a graphite die at 1450° C in argon atmosphere. X-ray analysis has confirmed that the composites are made of an alumina matrix and metallic chromium particles. Chromium has been chosen due to the direct reduction of chromium oxide by aluminium leading to metallic chromium and alumina as outlined above. The complete solubility of Al_2O_3 and Cr_2O_3 is favourable to obtain highly dense composites with

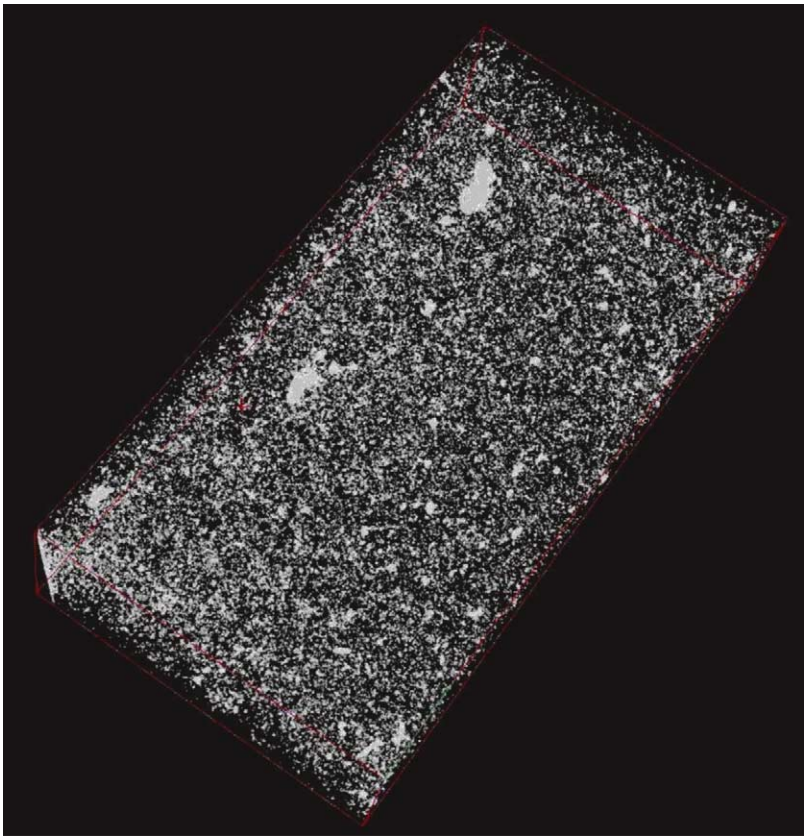

Fig. 2. X-ray microtomography of a composite containing 21 vol.% of chromium, volume size: 408 μm ×800 μm ×151 μm.

strong interfaces. No measurements have been made to evaluate interface strengths: this kind of experiments would be very complex on these particular microstructures. We have assumed that the strength of the interface is high because no particle decohesion has been observed during SEM or tomographic analysis (perhaps because of their small sizes) and also in considerations of the particular processing routes which was followed, involving in situ oxide metal reaction that yields fresh, presumably cleaner interfaces as compared to more conventional straight hot pressing.

Four types of samples have been used for this study. For the first three types, only the volume fraction of chromium has been modified, keeping the processing route unchanged: the chromium amount was 9, 21 and 36 vol.%. For the last sample, we kept a chromium volume fraction of 36%, modifying the processing route. Our usual processing is mechanical alloying consisting of four cycles of one hour at a speed of 360 rpm with 15 min break. The modified route consists of 16 cycles of 15 min at 360 rpm and 15 min break and, during these breaks, powders are scraped from the jar surface. The samples with 36% volume fraction of chromium thus will be called 36% type I for "usual" route and 36% type II for the modified route.

Dense composite microstructures, observed by the Scanning Electron Microscope (SEM) back scattered mode, are shown on Fig. 1. The metallic phase (in white on images) is dispersed in the alumina matrix. Chromium particles have complex shapes and wide size distributions. A few percent of residual porosity is also to be noted, a part of these porosites are due to alumina grain pull out during polishing. Using Archimedes' method, the amount of porosity in the composites has been estimated to be less than 3%.

This overall architecture bas been confirmed by X-ray tomography images such as that on Fig. 2, where we can see a homogenous dispersion of small particles with some of large size.[5] The size distribution has been determined by image processing. Fig. 3 shows the corresponding data for the different samples. From this figure, it appears that modifying the volume fraction of chromium has a direct influence on the size distribution, and modification of the processing route can also be used to alter this distribution. By adjusting the relative proportion of particles of different size, the microstructure in principle may be optimised with regards to residual stresses in the alumina matrix and the chromium particles, respectively. Because of the mismatch between thermal expansion coefficients of alumina and chromium,[6,7] alumina is globally under compression and chromium particles are in tension.[3,8] The existence of residual stresses in the matrix and particles may, due also to the shape of particles, lead to cracks being attracted by the particles, as pointed out by Ji and Yeomans.[9]

A more complete microstructural analysis of the alumina chromium composites can be found elsewhere.[3]

3. Experimental set-up—principle of Hertzian indentation

Several a priori criteria were thought appropriate for selecting an experimental procedure to investigate crack/microstructure interactions in the present composites.

- crack propagation must be stable.
- the crack geometry must be simple and single.
- the mechanical state produced by the external loading must be well defined, possibly analytically.
- a simple set-up to operate and a simple procedure to prepare test-samples.

From a literature review, it appears that Hertzian indentation meets all these criteria in our case. Other indentation methods raise some difficulties. Vickers or Knoop indentations have a more complicated geometry and multiple cracks occur during loading and unloading,[2] Single Edge Notched Beam (SENB) and Single Edge Precrack Beam (SEPB)

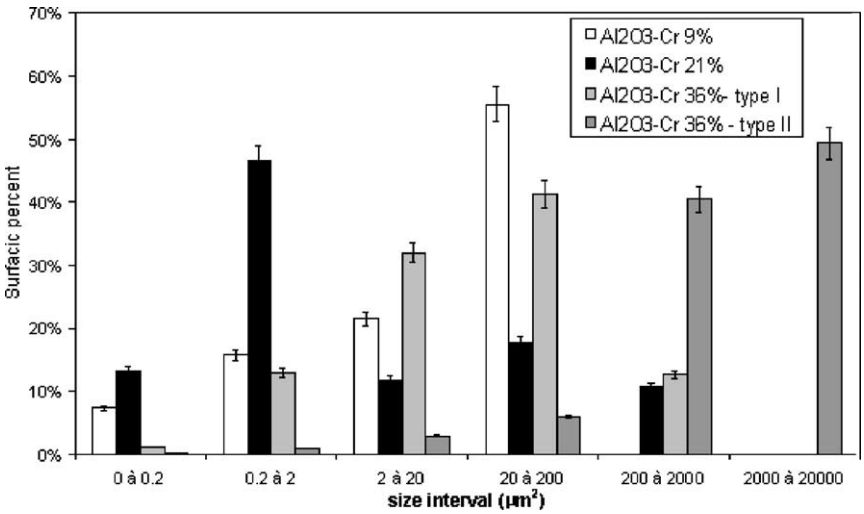

Fig. 3. Metallic particle size distributions (from SEM observations).

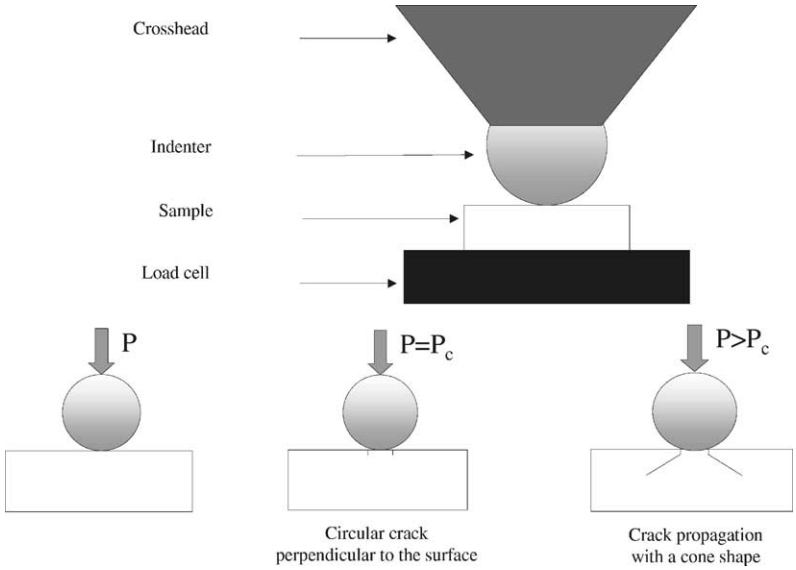

Fig. 4. Principle and experimental scheme of Hertzian indentation.

require delicate sample preparation.[10–15] The problems are similar when using flexion with pre-cracked samples,[16–19] the compact tension method[20–22] or the Double cantilever method.[23,24] The Miniaturized Disk-Bend Test is analogous to Hertzian but due to the sample size, analysis of crack propagation within the sample is not easy.[25,26] Advantages of Hertzian indentation include its well established basis.[27–29] Crack shape and stress field are well known for homogenous materials.[30–33] The determination of fracture toughness by this method has been applied to several ceramic[34–36] or glass materials.[32,37]

The principle of Hertzian indentation is to press a spherical indenter on the surface of a flat, well polished, sample. When the load reaches a critical value, a crack appears at the surface of the sample. This crack is circular due to the indenter geometry. If the load is increased over its critical value, the circular crack enters the sample and develops in the form of a conical crack, until loading ceases. Fig. 4 shows the different steps of the Hertzian indentation. In principle, no cracking is anticipated during unloading. But there may appear exceptions, e.g. in relation with particular ranges of loading/unloading rate.[38,39]

In the present work, indentations have been performed with a mechanical testing machine (Instron type 1185), operating in compression, with a load cell of 5 kN or 10 kN, depending on the sample, and a resolution of ±10 N and ±20 N, respectively. The displacement rate of the crossbeam was set to 1 μm or 2 μm per second up to a maximum load. This load was maintained for times of 1–50 s. Unloading has been programmed with a high speed of the crossbeam or with the same displacement velocity as during loading to assure the presence of a cone crack. Fig. 5 shows a typical loading cycle. These testing conditions are close to those usually reported in the literature.[31,32]

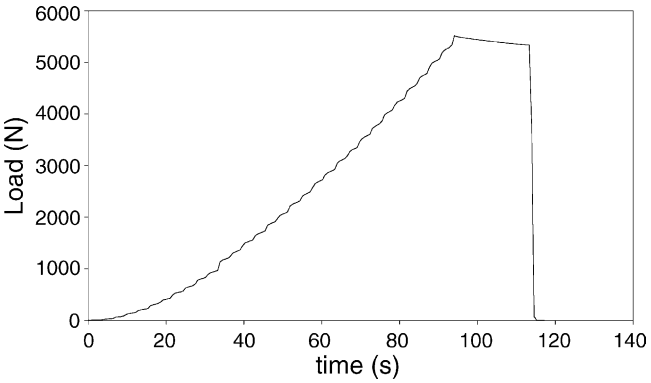

Fig. 5. Indentation cycle for alumina chromium composites.

Indenters made of WC-Co have been used (Young's modulus 628 GPa, Poisson's ratio 0.212 and radius 4 mm). This kind of indenters has been chosen for its mechanical properties similar to alumina/chromium composites, in order to reduce non-desirable effects, such as friction, that were identified during Hertzian test on float glass in a previous study.[40] After indentation, radii of the surface circular cracks were measured then samples were cut through the middle of the circular crack to observe the cone crack after polishing. The angle (measured with reference to the sample surface) and the length of the cone can then be measured, keeping in mind that the latter may be influenced by the cutting and polishing operations, as it will be discussed further below.

4. Results and discussion

In this section, we offer an analysis of the Hertzian crack in our composites at two scales. The first is a macroscopic scale, which is in accordance with the expected overall cone

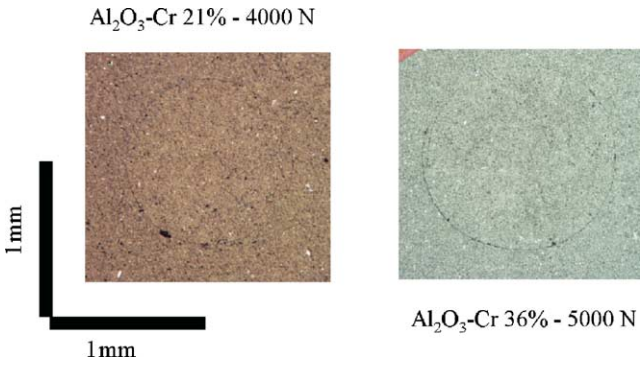

Fig. 6. Optical microscopy of circular surface crack.

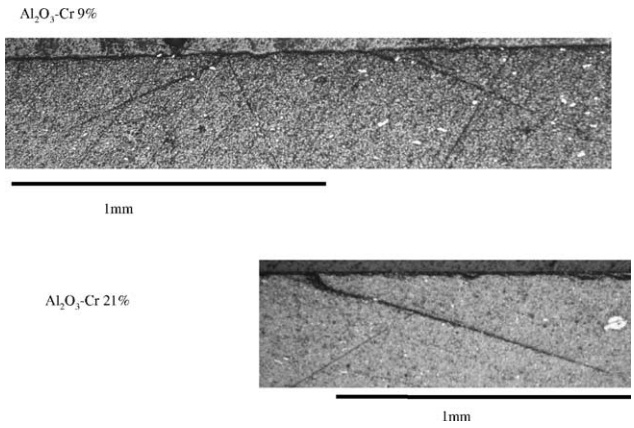

Fig. 8. Scanning electron microscopy of Hertzian cone crack.

crack geometry for seemingly homogenous materials and the second is the microscopic scale, where the microstructure level and heterogeneity come into play.

4.1. Macroscopic analysis—surface and cone crack analysis

Fig. 6 shows some views of the surface crack in different kinds of alumina chromium composites. Images show that a crack has a well defined circular shape and that its radius can be easily measured (this radius will be noted r_c in the analysis). The results of circular crack radius measurements are plotted on Fig. 7, versus applied load for these various types of composites. Also shown as straight lines on Fig. 7 are the corresponding radii of the contact area (noted a) as calculated from the following expression.[27,31,32,41]

$$a = \sqrt[3]{\frac{4kPR}{3E_2}} \quad \text{and} \quad k = \frac{9}{16}\left[\left(1-\nu_1^2\right)+\left(1-\nu_2^2\right)\frac{E_2}{E_1}\right]$$

where E is Young's modulus, ν is Poisson's ratio, P is the indentation load and R is the indenter radius, indexes 1 and 2 correspond to the indenter and sample, respectively.

For all kinds of composites, the measured crack radii are larger than the contact ones, as has been already noted in literature.[31,42,43] This effect confirms the fact that cracks initiate at a load value close to the maximum load applied to the sample and not in the first part of loading.

Typical examples of cone cracks in the alumina chromium composite are shown on Fig. 8. When examined at such low magnification, it seems that crack propagation was not disturbed by the sample microstructure. As a first approximation, it seems possible to rely on existing models for estimating the fracture toughness of the composites.

We followed two approaches which we previously validated for the case of float glass:[40] one based on the analy-

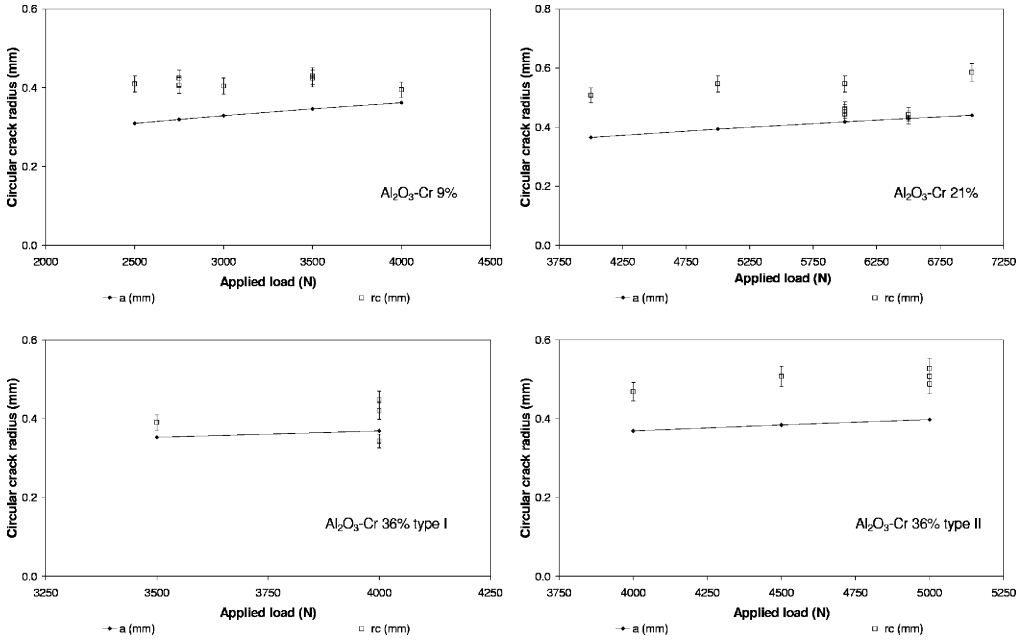

Fig. 7. Observed circular crack radius (r_c) and calculated contact radii (a) for the different samples.

Table 1
Fracture toughness estimation for alumina chromium composites

	Warren (minimum)	Warren (maximum)	Franck and Lawn
9%	6.9 ± 1.0	9.9 ± 1.0	6.1 ± 0.6
21%	7.8 ± 1.1	11.2 ± 1.1	7.2 ± 0.7
36% I	7.3 ± 1.2	10.6 ± 1.2	12.7 ± 1.2
36% II	7.8 ± 1.2	12.5 ± 1.2	13.0 ± 1.3

Minimum and maximum values of Warren's model correspond to $\beta = 1.1$ or 1.4, respectively.

sis of the surface circular crack, as proposed by Warren[37] and one based on the full cone crack analysis as proposed by Franck and Lawn.[30,43] Float glass has been used to test the Hertzian indentation because this materials is an industrial standard and has been studied by many authors using different techniques (Vickers indentation[13,18,44] or Hertzian test[31,32,37]) and the fracture toughness value is commonly assumed to be $0.75\,\mathrm{MPa\,m^{1/2}}$. A short reminder of the models is presented in Appendix A

Results for the fracture toughness of the composite are presented in Table 1, which shows that incorporating a metallic phase in the alumina matrix leads to an increase of the fracture toughness. Value for alumina must be taken as a reference, it corresponds to generally admitted fracture toughness for alumina with grain size of $1\,\mu\mathrm{m}$. This increase has also been observed by other techniques.[1] Values of fracture toughness values obtained by others authors on composites with equivalent (20%) chromium amount and similar processing techniques[1,9] are presented in Table 2.

From this figure, we can note that our fracture toughness estimated from Franck and Lawn's model and minimal value of Warren's model are of the same magnitude than those obtained by Vickers indentation and/or SENB and Vickers indentation.[1,9] Comparison of individual values from the different indentation tests, shows that using Warren's model provides relatively stable values whereas Franck and Lawn's model gives fracture toughness values which increase with the indentation load. This feature is a consequence of the model, as it relies on the stress field induced by the maximum load (see appendix).

Table 2
Comparison of alumina chromium composites fracture toughness with other equivalent composites[1,9]

Sample	Fracture toughness ($\mathrm{MPa\,m^{1/2}}$)
Pure Al_2O_3	4.0
Ji and Yeomans study[9] (Vickers indentation)	
SC Al_2O_3–Cr	5.0 ± 0.7
SF Al_2O_3–Cr	6.2 ± 0.8
HP Al_2O_3–Cr	7.1 ± 1.1
Guichard et al. study[1]—Al_2O_3–Cr 21%	
Using Vickers indentation	7.0 ± 0.4
Using SENB method	7.2 ± 0.0

Discussion about the two models[37,42] used for the fracture toughness determination are presented in Appendix B

As a consequence of the fracture toughness determination from two models, the fracture toughness of our alumina chromium composites determined here by Hertzian indentation may be considered as reasonable estimates rather than absolute values. A significant increase of mechanical properties of alumina due to the metallic phase is nonetheless confirmed and it is felt that Warren's model is closer to the real fracture toughness of the composites, because it is based on the circular crack at the surface. On the contrary, Franck and Lawn's model which relies on the analysis of the whole crack is sensitive to other effects as they have influenced the progressive development of the full cone crack. Such difficulties or artefacts would likely be similar if sharp indenters were used instead of spherical ones. Further work would be needed to clarify the corresponding issues.

4.2. Microscopic analysis

4.2.1. Crack-particle interaction

4.2.1.1. Observations of the crack path. If on the macroscopic scale, the crack path does not seem to be influenced by the metallic phase, the latter has an effect on the mechanical properties of composites as evidenced by their fracture toughness. Thus, upon closer examination of microstructures (Fig. 9) interactions between crack and particles become more evident. Various propagation cases can be identified from these observations, and are exemplified on Fig. 9. Beyond some distance from the main crack line no interaction is noticeable. However, when the crack runs close to a particle it may either reach it and possibly induce some deformation of the metal, or be deflected away possibly with some decohesion at the matrix/particle interface. Using image processing, we determined the sizes of both categories of particles. The results are presented on Fig. 10 and for comparison the size distributions of the entire populations are also shown. The composite with 9% of chromium is not reported due to poor statistics. For example, for this composite, the number of particles for which decohesion and deformation occur are 22 and 16, respectively. For the other composites, these numbers are between 200 and 360 particles for decohesion and 56 to 73 when deformation is detected. On Fig. 10, it may be noted that large particles have a greater tendency to be reached by the crack and deformed whereas smaller particles are more likely to be bypassed.

In addition to the size effect, observations made on SEM images point to an orientation effect of the chromium particles. When a particle is elongated in the direction of the crack propagation, the crack tends to bypass the particle and when the particle is elongated in the direction perpendicular to the crack propagation, the particle tends to be deformed.

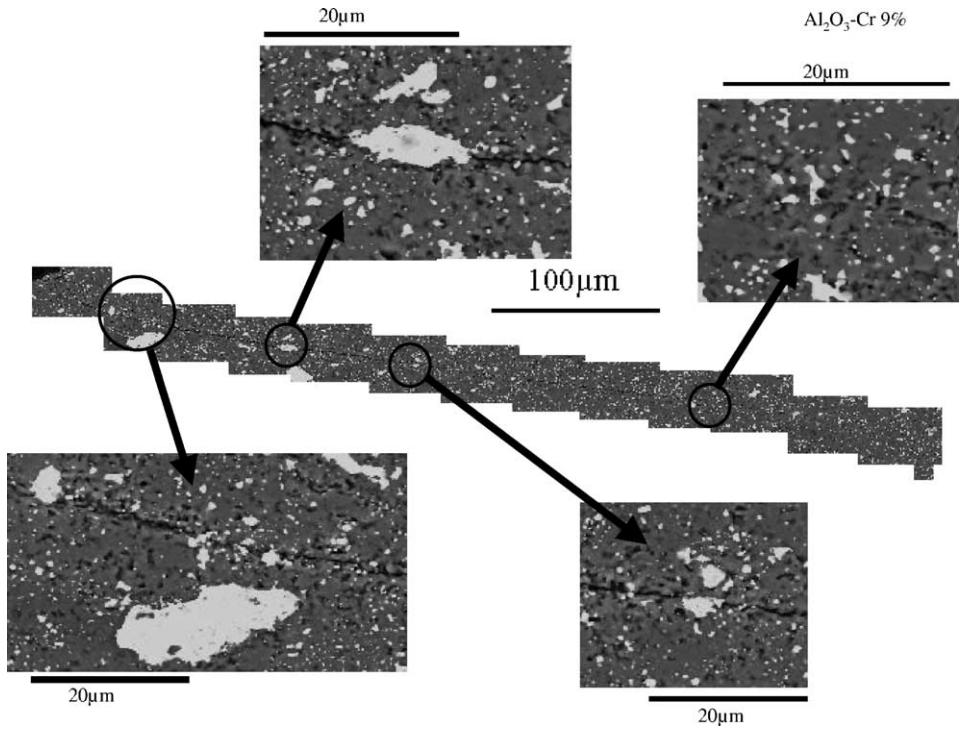

Fig. 9. SEM image of the crack path in a 9% chromium composite.

these features of crack/particle interactions may be rationalized as follows.

4.2.1.2. Micromechanical analysis. In previous studies[3,8] we have analysed the residual state of stress in the composites using a micromechanical approach. In order to study, the stress field evolution during Hertzian indentation, we have surperposed to this stress field, a stress field equivalent to the stress that develop in the microstructure during Hertzian indentation (as calculated from theory[31]). This approach is

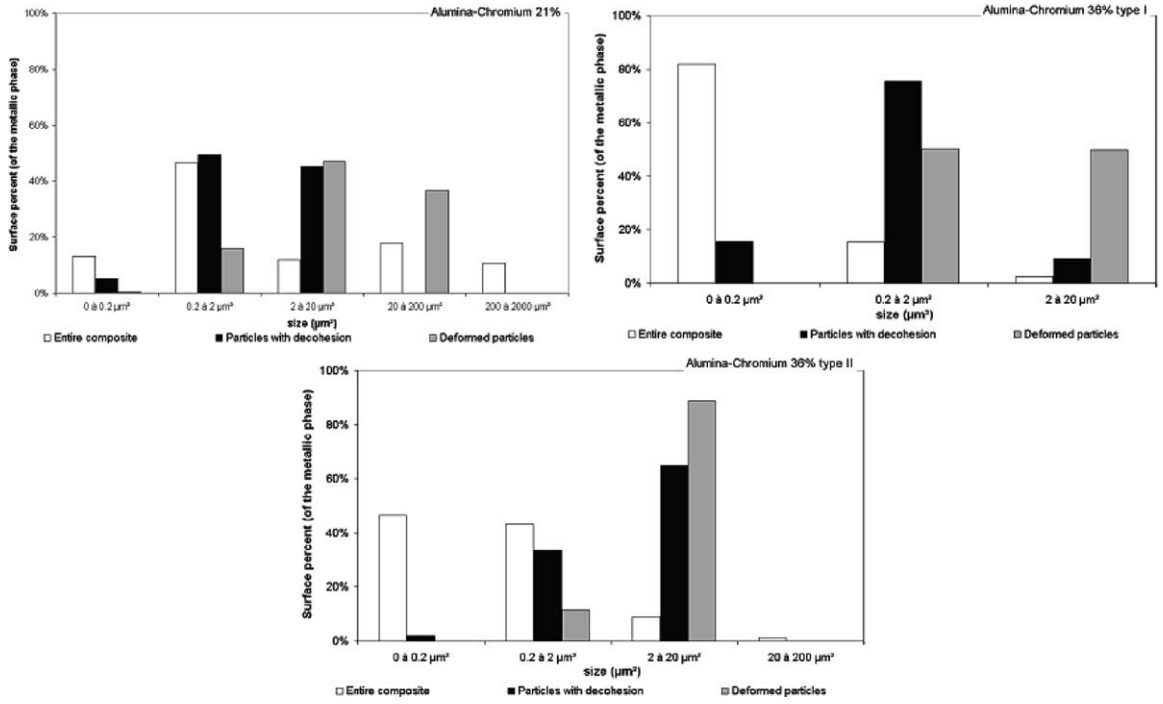

Fig. 10. Particles size distributions along cone cracks.

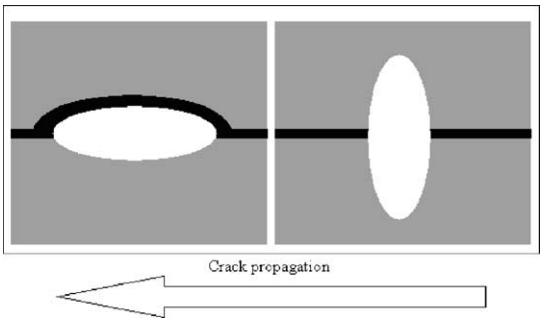

Fig. 11. Simple case of particle and crack interaction.

a strong simplification of the real case, so it must be taken as a first approach of the stress and crack behaviour in this particular microstructure. Using the cumulation of the two stress fields, it is possible to evaluate the orientation effect of particles on crack propagation. From microscopic observations, we have identified two limiting cases for particle orientation. We will consider metallic particles with ellipsoidal shape, which is more frequent for particles with size greater than the crack opening, these kind of particles can more easily interact with the crack. Conversely, the spherical shape is common for smaller particles. The two limiting cases which will be considered are schematically shown on Fig. 11. Assuming that crack propagation takes places in mode I under the effect of Hertzian load and residual stresses in alumina–chromium composites, we have also assumed Hertzian loads close to those used during experiments, typically up to 1000 MPa. For calculations, we used three dimensional models representing an ellipsoidal metallic particle in the matrix. External faces of the cell are supposed to be free to deform and the volume of the particle represents 3.5% of the entire cell. Let us recall that the major results from the micromechanical model without external load, is that chromium particles are in tension and alumina in compression and that stress levels are dependant upon volume fraction and particle shape.[3,8]

Here we only are interested in profiles, corresponding to the stress responsible for mode I propagation. The profiles are plotted along a symmetry axis of the particles. So, for the particle oriented along the crack direction, σ_{11} is shown in Fig. 12 and σ_{33} in Fig. 13 for the particle oriented in the perpendicular direction, respectively. The crack is supposed to propagate from right to left on both figures. See Ref. [3] for more details on the calculations.

Fig. 12 corresponds to a case where some decohesion at the interface appears. Under no applied load, the alumina matrix is in compression and the level of compression is maximum at the metal–ceramic interface. When the applied load is increased, away from the particle, the stress becomes tensile hence favourable to crack propagation. But in the vicinity of the interface, for low load levels, the stress is still compressive which yields to crack deviation.[45] When the load reaches higher levels, σ_{11} is tensile in the matrix, but near the interface, the level remains lower than the one far from the particle. Therefore, in this case, the stress level in the particle has no influence on crack propagation because the crack does not reach the particle, and is deflected as suggested by experimental observation (Fig. 9).

On the other hand, when the particle is elongated in the perpendicular direction to the crack propagation, experimental observations are indicative of deformation of the particle rather than decohesion at the interface. The stress profile on Fig. 13 shows that in the absence of external load, alumina is in compression. With the increase of load, the stress in the matrix becomes tensile with higher level near the interface than at the cell boundary. When the crack is propagating, the tensile stress field is favourable to its propagation and in that case the crack reaches the particle. As the stress level in the particle is high and in tension, the particle can be deformed.

A similar analysis can be made with particles of concave shape. In previous work,[3,8] we have shown that when a particle has a concave shape and when chromium has an elastoplastic behaviour, the matrix becomes tensile in the concavity. This region with tensile stress is favourable for particle deformation, as concavities on the metallic particles may be seen as traps for cracks.

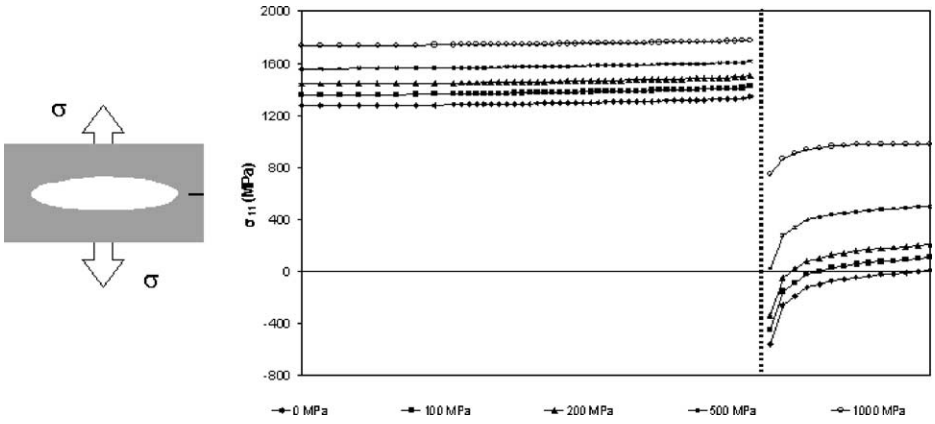

Fig. 12. σ_{11} stress profile on the major axis of the ellipsoid for different applied loads.

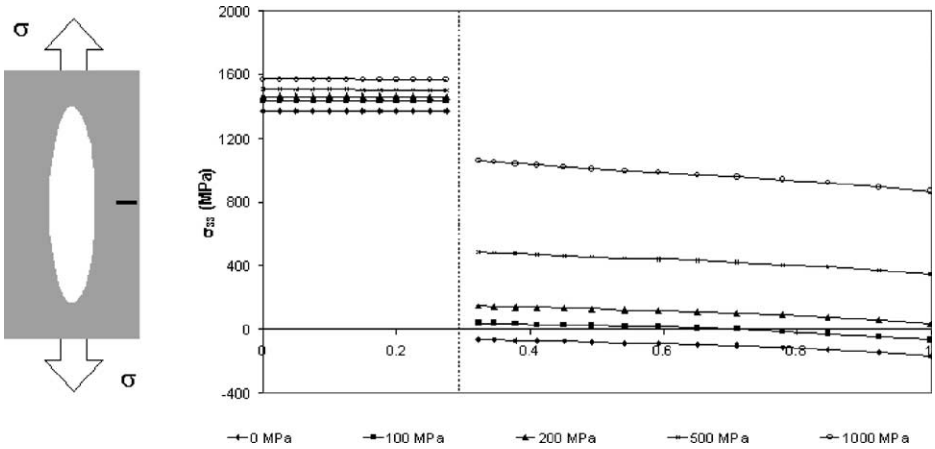

Fig. 13. σ_{33} stress profile on the minor axis of the ellipsoid for different applied loads.

4.2.2. Crack trajectory

Bearing in mind this crack/particle interactions we may before closing consider again the overall cone crack paths.

As mentioned, the average value of cone angle is 20°, in all of our composites, with extremes of 15° and 25°. In the literature, two approaches have been used to estimated the cone angle. One by Lawn et al.[46] who calculated the cone angle from the theoretical stress field, and another one by Kocer and Collins[47] who considers the crack trajectory to results from a maximum energy release rate criterion, in accordance with an advanced stress field evolving with crack propagation. Here, we have simulated the crack trajectory from the Hertzian stress field using a maximum energy release rate criterion, but with less sophistication than Kocer in that no relaxation of the initial stress field during crack advance is provided for (see Appendix C). Fig. 14 shows typical examples of real crack trajectories observed in the composites, and the corresponding simulated ones.

Again, two kinds of situations can be identified:

- If particles of large size are present close to the crack trajectory and are suitably oriented with respect to the crack direction, their stress field[8] induces a change in such direction. Subsequently, after overriding or bypassing the particle, the crack tends to recover its previous orientation.
- If no particle of large size is present close to the crack trajectory, then the latter matches the simulated one, as in the case of the crack in the 9% composite (trajectory (2) on Fig. 14a).

Considering its simplicity, our simulation may be expected to yield results somewhat at variance with experiment, even for the ideal case of a single phase homogeneous material[46,47] not with standing the presence of chromium inclusions. However, when no large particles are present in the vicinity of the propagating crack, both simulation and experiment are not too far apart, it being kept in mind that the former is represented on a diametral plane, whereas the plane of observation may be off-centered due to sample preparation.

Such discrepancies between simulations and observations may also be estimated in terms of differences in the respective crack opening σ_1 stress levels. thus, for the 9% composite (Fig. 14a) the ≈40 MPa difference in the favourable case becomes ≈350 MPa in the vicinity of the large particles; i.e. about 50% of the applied indentation stress, decreasing again to ≈20% beyond them, when the crack straightens out again. Similar behaviours are noted for higher chromium volume fractions (Fig. 14b) but more pronounced since indentation stress levels also are higher. In summary, the preceding discussion shows that qualitatively at least the maximum energy release rate criterion adequately describes crack propagation at sufficient distance from large particles whereas close to the particle, their associated stress fields

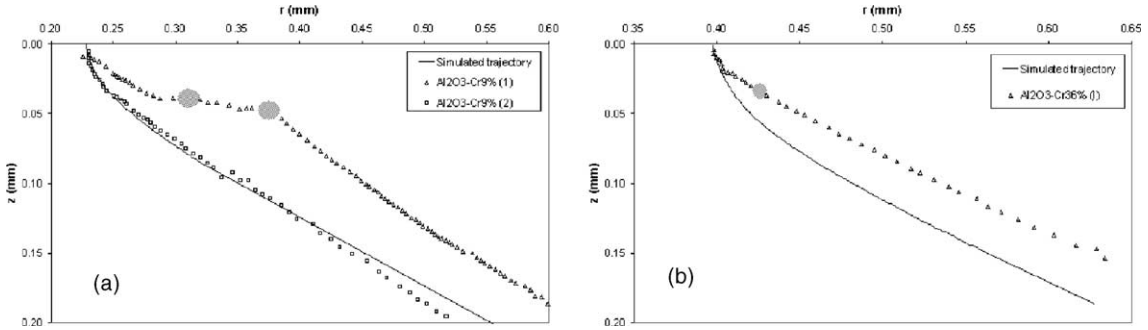

Fig. 14. Comparison of simulated and real trajectory in alumina chromium composites. Ellipsoidal mark indicates positions of large particles.

Table 3
Crack length and bandwidth for the different samples

Chromium volume fraction	Crack length (μm)	Bandwidth (μm)
9%	80	4.00
	288	6.40
	354	8.57
	463	8.18
21%	174	1.74
	243	3.48
	558	12.56
36% I	116	2.58
	671	8.39

may become dominant over the externally applied Hertzian stress,[8] inducing some wandering in the crack trajectory. This effect may be quantified via the definition of an envelope in which the crack path is seen to fluctuate. The corresponding bandwidth of this envelope has been estimated at various distances down from the outer surface (Table 3), and it seems to increase with the overall crack length, consistent with the fact that the applied Hertzian stress tends to decrease with depth into the sample to eventually become comparable or even smaller than local large particle residual stresses.

5. Conclusion

Using Hertzian indentation on alumina chromium composites, we have identified the principal parameters that characterise crack development in relation with the microstructure. Improvement of the mechanical properties of alumina by metallic particle addition has been assessed by estimating the fracture toughness from a macroscopic analysis of the crack. From a microscopic analysis of the crack, the importance of particle size distribution has been evidenced.

Using micromechanical calculations, we have analysed the influence of the local stress field around the particles on the crack propagation and shown that the behaviour of the crack is influenced by such stress field, itself depending upon particle shape and orientation. For the sake of simplicity, calculations have assumed alumina and chromium to be pure, with elastic and elastoplastic behaviours, respectively. Reality is somewhat more complex chemically speaking, and a more detailed analysis carried out elsewhere[3] has shown that in all cases, the calculated residual stress levels and evolutions are accurate within 10%.

The micromechanical approach correlated with the microstructure analysis can be used to rationalize results obtained on other composites of similar nature. For example, Sun and Yeomans[48] have investigated the fracture toughness of Al_2O_3–Ni composites with various microstructures. They found that composites with rough interfaces have higher fracture toughness than composites containing metallic particles with regular shapes. The increase of fracture toughness due to the former type of microstructure could have been anticipated. The mechanical properties of nickel and chromium are rather similar, thus the stress fields should have similar distributions. According to our calculations, it can be predicted that the crack will be trapped by the particles with rough interface, the tendency for these particles to dissipate energy by deformation is higher, so fracture toughness of the composite is increased, as in our case.

In summary, the present work is believed to have brought to evidence some essential microstructural parameters on features governing crack propagation; i.e. particle size, orientation and shape, with some quantification of their respective effects. Some basis for designing improved, if not optimal, microstructures leading to high fracture toughness is now available, and possibly applicable to a whole range of ceramic–metal composites.

Acknowledgements

We wish to thank Jean-Marie Hiver, at L.P.M. (Ecoles des Mines de Nancy), for his help during indentation tests.

Appendix A. Models for fracture toughness determination with Hertzian crack

In Warren's approach,[37] fracture toughness is obtained from the following formula:

$$K_{\mathrm{Ic}} = \left(\frac{E^* P_{\min}}{P_{\mathrm{FN}}^{\min} R}\right)^{1/2} \quad \text{where} \quad \frac{1}{E^*} = \frac{1-\nu_2^2}{E_2} + \frac{1-\nu_1^2}{E_1}$$

where, R is the indenter radius, $P_{\min}$ is the minimal load for surface crack propagation and $P_{\mathrm{FN}}^{\min}$ is a constant depending on the sample and indenter mechanical properties.[37] In our set-up, the determination of $P_{\min}$ is not easy, due the poor resolution of the test machine. As the surface crack appears in a range of 1.1–1.4 time the contact area,[28,31,42] we estimated $P_{\min}$ for these two values on starting radii.

$$P_{\min} = \frac{3E_{\mathrm{sample}}a^3}{4kR} \text{ with } a = \frac{r_{\mathrm{c}}}{\beta} \quad \text{and} \quad \beta = 1.1 \text{ or } 1.4$$

where r_{c} is the radius of the surface crack.

In Franck and Lawn's model, fracture toughness is determined by:

$$K_{\mathrm{Ic}} = 2\left(\frac{c_0}{\pi}\right)^{1/2} \int_0^{c_0} \frac{\sigma_1(c)}{\left(c_0^2 - c^2\right)^{1/2}} \mathrm{d}c$$

where c_0 is the cone crack length and σ_1 is the first principal stress along the crack.

The fracture toughness determination by both models, particularly Franck and Lawn's one requires the knowledge of the mechanical state in the composite. This mechanical state

Table A.1
Mechanical properties of alumina chromium composites

Sample	Young's modulus (GPa)	Poisson's ratio	P_{min}^{FN}
Al_2O_3	402	0.25	2539
Al_2O_3–9%	389	0.25	2539
Al_2O_3–21%	374	0.24	2457
Al_2O_3–36% I and II	356	0.24	2367
WC–Co (indenter)	628	0.21	2069

can be calculated by a system of equations[31,46,49] using the mechanical properties of the composites. These properties were determined by ultrasonic methods[4] and are presented in Table A.1.

Appendix B. Models discussion

The precise determination of the fracture toughness of alumina chromium composites is delicate. From the experimental point of view, there exist different error sources for both models. For example, our number of data points is less than the 25 test values recommended by Warren[37] in order to reach accurate enough P_{min} values. Due to the resolution of the testing machine, no effect on the load curve due of the crack propagation could be detected. For Franck and Lawn's model, errors come from the determination of the crack length and crack angle. As our samples are not transparent, they have been cut for the measurement. This operation can trigger further crack propagation, possibly outlined by some cone angle modification along the crack.

Another source of error comes from the calculation of the mechanical state. The calculations are extremely dependent on the sample and indenter mechanical properties, by way of the constant P_{FN}^{min} in Warren's model or the σ_1 stress in Franck and Lawn's model. As the crack is principally located in the matrix, we have quantified this effect by using the mechanical properties (Young's modulus and Poisson's ratio) of pure alumina instead of the ones of composites for the Franck and Lawn's model. The calculation made with the mechanical properties of the composites lead to a difference on the fracture toughness of 3% for the 9 vol.% composite, 9% and 15% for the composite containing 36% type I and II, respectively.[3]

The Franck and Lawn model also depends upon the cone crack angle. In our composite this angle is not truly constant as in the case of homogenous materials such as glass. For example, the cone angle is 20° and 17° for the 9 and 21 vol.% composites, respectively. As the mechanical properties of the sample are very close (see Table A.1), smaller variations on the cone angle would have been expected. This variation may be in relation with the microstructure of the composite and its influence on the onset of crack propagation.

Another effect that can modify the fracture toughness value is friction between indenter and sample.[41] If both have different mechanical properties, it may lead to an overestimation of the fracture toughness when the Poisson's ratio of the sample is lower than the one of the indenter. Conversely, the fracture toughness could be underestimated in our case.

The external loading rate can also have an influence on the determination of the fracture toughness. In this study, no significant modification of the behaviour was noted when using different loading rates on the composites, although subcritical or slow cracking can not be ruled out. Thus $\dot{P}$ has not been taken into account in this work, but it can have an influence on crack propagation due to the existence of a relation between $\dot{a}$ and $\dot{P}$.[50] This relation implies that at constant load rate, as in our case, the contact area radius rate decreases with time to be nearly constant when the maximum load is reached, as highlighted by Fig. B.1. Since

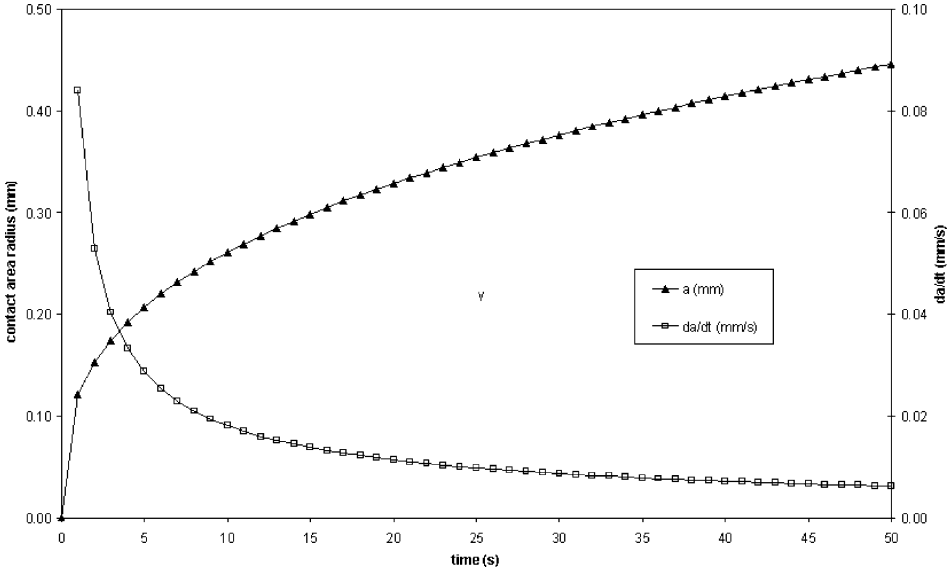

Fig. B.1. Evolution of contact area radius and rate vs. time.

at the same time, the cone surface increases, then a decrease of the crack propagation rate may result. But this effect has not been further investigated in the present work.

Finally, although it is generally admitted that fully dense fine grain size (≈1 μm) alumina has a single valued toughness or in other words, does not exhibit R-curve effect,[51] such a behaviour has been observed in composites such as ours using other techniques (Vickers indentation and DCB).[1,9] Evaluation of the R-curve behaviour is difficult in the case of Hertzian indentation because the sample needs to be cut for the observation of the crack, contrary to DCB or Vickers indentation, and the cut can result in an overestimation of the crack length, as already mentioned. Neither has R-curve behaviour been experimentally assessed in the present work.

Appendix C. Crack trajectory simulation during Hertzian contact

During an Hertzian contact, in the Franck and Lawn's model,[30,43] crack is propagating along the σ_3 principal stress perpendicular to the σ_1 principal stress. Our simulation are based on the following assumptions:

(i) the presence of the crack does not disturb the stress field.
(ii) the cone crack develops with a σ_1 principal stress always normal to the crack trajectory.
(iii) the initial surface crack can be neglected in regard to its size versus the cone length.

If this model is sufficient to estimate the fracture toughness of samples, it is not quite satisfactory to calculate the crack trajectory. As a matter of fact, from the stress field, it is normally possible to estimate the angle of the cone crack and so to determine the trajectory. But results on angle and trajectory are not consistent and it is necessary to modify, for example, the Poisson's ratio of the sample to deduce, from the stress field, an angle in agreement with experimental results.[46]

Other authors[47] use other criteria in finite element models. The crack propagates in order to yield the maximum energy release rate and the stress field is evolving with the crack propagation, i.e. the stresses are relaxed along the crack. With this model, the results are very close to observations on glass samples.

In the case of alumina chromium composites, we have used a criterion based on the maximum energy release rate in combination with the stress field given by Franck and Lawn. In the model, the energy release rate is calculated by the formula:

$$G = \frac{K_{\mathrm{I}}^2}{E} + \frac{1+\nu}{E}K_{\mathrm{II}}^2 + \frac{1+\nu}{E}K_{\mathrm{III}}^2$$

where K_{I}, K_{II} and K_{III} are the stress intensity factors in mode I, II and III, respectively, and E and ν are the Young's modulus and Poisson's ratio of the sample. In the Hertzian theory, stress fields are expressed in the symmetry plane of the contact area, so mode I is calculated using the first principal stress σ_1, mode II using the shear stress τ_{zr} and the mode III is nil. In our model, stress intensities are calculated using the formalism developed by Franck and Lawn:

$$K_{\mathrm{I}} = 2\left(\frac{c_0}{\pi}\right)^{1/2}\int_0^{c_0}\frac{\sigma_1}{(c_0^2-c^2)^{1/2}}\mathrm{d}c \quad \text{and}$$

$$K_{\mathrm{II}} = 2\left(\frac{c_0}{\pi}\right)^{1/2}\int_0^{c_0}\frac{\tau_{zr}}{(c_0^2-c^2)^{1/2}}\mathrm{d}c$$

Calculations are carried out along the whole crack.

For the trajectory calculation, to determine the point where the energy release rate is maximal, we use the following procedure:

- We place a flaw on the surface, near the contact area, with a very small size compared to the cone length (Fig. C.1a). Typically, the size is the same as the crack increment, of the order of 1 μm.
- A fixed indentation load is applied to the sample on the spherical indenter. The stress field induced by this load is known.
- Energy release along the flaw is calculated for the applied load.
- At the crack tip, in a solid angle Ω, different possible orientations for a fixed crack increment, are tested and the energy release rate is compared to the previous one in order to find the maximum (Fig. C.1b).
- Crack size is incremented in accordance to the maximum of G. The new energy release rate, corresponding to the

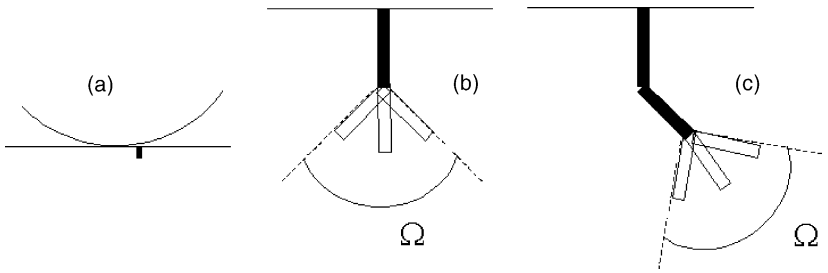

Fig. C.1. Model for crack propagation: (a) initial position, (b) first increment of the crack, (c) second increment.

incremented crack, is calculated and the operation is iterated at the new crack tip (Fig. C.1c).

- The external load is incremented to propagate the crack.

References

1. Guichard, J. L., Tillement, O. and Mocellin, A., Alumina chromium cermets by hot pressing of nanocomposites powders. *J. Eur. Ceram. Soc.* 1998, **18**, 1743–1752.
2. Whittle, B. R. and Hand, R. J., Morphology of vickers indent flaws in soda lime silica glass. *J. Am. Ceram. Soc.* 2001, **84**(10), 2361–2365.
3. Geandier, G., *Relation entre la microstructure, l'état mécanique et la fissuration de cermets alumine chrome élaborés à partir de poudres nanocomposites*. Ph.D. thesis, Institut National Polytechnique de Lorraine, Nancy, 2002.
4. Guichard, J. L., *Elaboration et caractérisation de cermets alumine-métal àpartir de poudres obtenues par mécanosynthèse*. Ph.D. thesis, Institut National Polytechnique de Lorraine, Nancy, 1998.
5. Geandier, G., Denis, S., Hazotte, A., Mocellin, A. and Maire, E., Microstructural analysis of alumina chromium composite by X-ray tomography and 3-D finite element simulation of thermal stresses. *Scr. Mater.* 2003, **48**, 1219–1224.
6. Touloukian, Y. S., Kirby, R. K., Taylor, R. E. and Desai, P. D., Thermal expansion: metallic elements and alloys. In *Thermophysical Properties of Matter, Vol 12*. NY, Washington, 1970, pp. 61–67.
7. Touloukian, Y. S., Kirby, R. K., Taylor, R. E. and Desai, P. D., Thermal expansion: metallic elements and alloys. In *Thermophysical Properties of Matter, Vol 12*. NY, Washington, 1970, pp. 176–185.
8. Geandier, G., Weisbecker, P., Denis, S., Hazotte, A., Mocellin, A., Lebrun, J. L. *et al.*, X-ray diffraction analysis of residual stresses in alumina–chromium composites and comparison with numerical simulations. In *Materials Science Forum, Vols 404–407*. Trans Tech Publications, Switzerland, 2002, pp. 547–552.
9. Ji, Y. and Yeomans, J. A., Microstructure and mechanical properties of chromium and chromium/nickel particulate reinforced alumina ceramics. *J. Mater. Sci.* 2002, **37**, 5229–5236.
10. Nishida, T. and Kameyama, I., Evaluation of fracture toughness for structural ceramics using SEPB specimens (part 4)—fracture behavior of α-alumina polycristals with different grain sizes. *J. Ceram. Soc. Jpn. Int. Ed.* 1991, **100**, 288–294.
11. Sorensnen, B. F., Horsewell, A., Jorgensen, O. and Kumar, A. N., Fracture resistance measurement method for in situ observation of crack mechanisms. *J. Am. Ceram. Soc.* 1998, **81**(3), 661–669.
12. Gogotsi, G. A. and Galenko, V. I., Comparative analysis of fracture toughness test methods for ceramics and crystals at room and lower temperature. *Strength Mater.* 1997, **29**(3), 287–297.
13. Anstis, G. R., Chantikul, P., Lawn, B. R. and Marshall, D. B., A critical evaluation of indentation techniques for measuring fracture toughness: I. Direct crack measurement. *J. Am. Ceram. Soc.* 1981, **64**(9), 533–538.
14. Ponton, C. B. and Rawlings, R. D., Vickers indentation fracture toughness test: Part 1. Review of literature and formulation of standardized indentation toughness equations. *Mater. Sci. Technol.* 1989, **5**, 865–872.
15. Ponton, C. B. and Rawlings, R., Vickers indentation fracture toughness test: Part 2. Application and critical evaluation of standardized indentation toughness equations. *Mater. Sci. Technol.* 1989, **5**, 961–976.
16. Krauss, R. F., Rising fracture toughness from the bending strength of indented alumina beams. *J. Am. Ceram. Soc.* 1988, **71**(5), 338–343.
17. Swain, M. V., Comparison of K_{1C} values for Al_2O_3–ZrO_2 composites obtained from notched-beam and indentation strength techniques. *Commun. Am. Ceram. Soc.*, 1983, 27–29.
18. Anstis, G. R., Chantikul, P., Lawn, B. R. and Marshall, D. B., A critical evaluation of indentation techniques for measuring fracture toughness: II. Strength method. *J. Am. Ceram. Soc.* 1981, **64**(9), 539–543.
19. Murphy, B. R., Predebon, W. W. and Pletka, B., The fracture toughness of a high strength alumina: compact tension versus indentation fracture techniques. *J. Mater. Sci. Lett.* 1994, **13**, 1346–1348.
20. Densley, J. M. and Hirth, J. P., Fracture toughness of a nanoscale WC-Co tool steel. *Scr. Mater.* 1998, **18**(2), 239–244.
21. Raddatz, O., Schneider, G. A. and Claussen, N., Modeling of R-curve behavior in ceramic metal composites. *Acta Mater.* 1998, **46**(18), 6381–6395.
22. de With, G. and Sweegers, N., Small specimen compact tension testing of ceramics. *J. Mater. Sci. Lett.* 1994, **13**, 1038–1041.
23. Bradt, R. C., Hasselman, D. P. H. and Lange, F. F., *Fracture Mechanics of Ceramics: Concepts, Flaws and Fractography, Vol 1*. Plenum Press, New York, 1974 (iSBN 0-306-375931-5 (v. 1)).
24. Trusty, P. A. and Yeomans, J. A., Crack particle interactions in alumina iron composites. In *Ceramic Engineering and Sciences Proceedings, Vol 14*, 9–10, 1993, pp. 908–913.
25. Li, H., Chen, F. C. and Ardell, A. J., A simple, versatile miniaturized disk bend test apparatus for quantitative yield stress measurement. *Metall. Trans. A* 1991, **22A**, 2061–2068.
26. Meyers, D. E., Chen, F. C., Zhang, J. and Ardell, A. J., Optimization of test parameters for quantitative stress measurement using the miniaturized disk bend test. *J. Testing Eval.*, 1993, 263–271.
27. Hertz, H., *Hertz's Miscellaneous Paper*, Macmillan, London, 1896, Chapters 5 and 6.
28. Auerbach, F., Absolute hortemessung. *Ann. Phys. Chem.* 1891, **43**, 61.
29. Huber, M. T., Zur theorie der berhrung fester elasticher körper. *Ann. Phys.* 1904, **14**, 153.
30. Lawn, B. R., Hertzian fracture in single crystals with the diamond structure. *J. Appl. Phys.* 1968, **39**, 4828–4836.
31. Zeng, K., Breder, K. and Rowcliffe, D. J., The Hertzian stress field and formation of cones cracks—I. Theoretical approach. *Acta Metall. Mater.* 1992, **40**(10), 2595–2600.
32. Zeng, K., Breder, K. and Rowcliffe, D. J., The Hertzian stress field and formation of cones cracks—II. Determination of fracture toughness. *Acta Metall. Mater.* 1992, **40**(10), 2601–2605.
33. Lawn, B. R., Padture, N. P., Cai, H. and Guiberteau, F., Making ceramics ductile. *Science* 1994, **263**, 1114–1116.
34. Laugier, M. T., Load bearing capacity of tin coated WC-Co cemented carbides. *J. Mater. Sci. Lett.* 1983, **2**, 419–421.
35. Carroll, I., Sternitze, M. and Derby, B., Silicon carbide particle size effects in alumina based nanocomposites. *Acta Mater.* 1996, **44**(11), 4543–4552.
36. Laugier, M. T., Toughness determination of some ceramic tool materials using the method of Hertzian indentation fracture. *J. Mater. Sci. Lett.* 1985, **4**, 1542–1544.
37. Warren, P. D., Determining the fracture toughness of brittle materials by Hertzian indentation. *J. Eur. Ceram. Soc.* 1995, **15**, 201–207.
38. Lawn, B. R., An atomistic model of kinetic crack growth in brittle solids. *J. Mater. Sci.* 1975, **10**, 469–480.
39. Lagitan, F. B. and Lawn, B. R., Effect of a reactive environment on the Hertzian strength of brittle solids. *J. Appl. Phys.* 1970, **41**(6), 3357–3365.
40. Geandier, G., Denis, S. and Mocellin, A., Float glass fracture toughness determination by Hertzian contact: experiments and analysis. *J. Non-Cryst. Solids* 2003, **318**, 284–295.
41. Johnson, K. L., O'Connor, J. J. and Woodward, A. C., The effect of the indenter elasticity on the Hertzian fracture of brittle material. *Proc. R. Soc. Lond.*, 1973, **A334**, 95–117.
42. Warren, R., Measurement of the fracture properties of brittle solids by Hertzian indentation. *Acta Metall.* 1978, **26**, 1759–1769.
43. Frank, F. C. and Lawn, B. R. On the theory of Hertzian fracture. *Proc. R. Soc.*, 1967, **A229**, 291.

44. Bourhis, E. L. and Metayer, D., Indentation of glass as a function of temperature. *J. Non-Cryst. Solids* 2000, **272**, 34–38.
45. Genevrier, M., *Synthèse et propriétés mécaniques de composites de cordiérite. un nouveau modèle de déviation de fissure*. Ph.D. thesis, Institut National Polytechnique de Lorraine, Nancy, 1992.
46. Lawn, B. R., Wilshaw, T. R. and Hartley, N. E. W., A computer simulation study of Hertzian cone crack growth. *Int. J. Fract*. 1974, **10**(1), 1–16.
47. Kocer, C. and Collins, R. E., Angle of Hertzian cone cracks. *J. Am. Ceram. Soc.* 1998, **81**(7), 1736–1742.
48. Sun, X. and Yeomans, J. A., Optimization of a ductile particle toughened ceramic. *J. Am. Ceram. Soc.* 1996, **79**(10), 2705–2717.
49. Fischer-Cripps, A. C., Predicting Hertzian fracture. *J. Mater. Sci*. 1997, **32**, 1277–1285.
50. Lawn, B. and Wilshaw, R., Review. Indentation fracture: principles and applications. *J. Mater. Sci*. 1975, **10**, 1049–1081.
51. Braun, L. M., Benisson, S. J. and Lacou, B. R., Objective evaluation of short crack toughness curves using indentation flaws: case study on alumina based ceramics. *J. Am. Ceram. Soc.* 1992, **75**(11), 3049–3057.